A Continuous-Flow, Microfluidic Fraction Collection Device

Christopher Baker and **Michael G. Roper**[*]

Department of Chemistry and Biochemistry, Florida State University, 95 Chieftain Way, Tallahassee, FL 32306, USA

Abstract

A microfluidic device is presented that performs electrophoretic separation coupled with fraction collection. Effluent from the 3.5 cm separation channel was focused via two sheath flow channels into one of seven collection channels. By holding the collection channels at ground potential and varying the voltage ratio at the two sheath flow channels, the separation effluent was directed to either specific collection channels, or could be swept past all channels in a defined time period. As the sum of the voltages applied to the two sheath flow channels was constant, the electric field remained at 275 V/cm during the separation regardless of the collection channel used. The constant potential in the separation channel allowed uninterrupted separation for late-migrating peaks while early-migrating peaks were being collected. To minimize the potential for carryover between fractions, the device geometry was optimized using a three-level factorial model. The optimum conditions were a 22.5° angle between the sheath flow channels and the separation channel, and a 350 µm length of channel between the separation outlet and the fraction channels. Using these optimized dimensions, the device performance was evaluated by separation and fraction collection of a fluorescently-labeled amino acid mixture. The ability to fraction collect on a microfluidic platform will be especially useful during automated or continuous operation of these devices or to collect precious samples.

Keywords

microfluidic; fraction collection; electrophoresis; separation

1. Introduction

One of the primary advantages presented by microfluidic devices is the degree with which processes can be integrated and automated. There have been multiple examples of devices which have integrated a large number of sample handling steps, for example, in material synthesis [1], single cell analysis [2], and DNA analysis [3]. Microfluidic devices are also amenable to automating processes in a simple and low-cost manner. Examples of automated microfluidic devices include long-term monitoring [4], preparative separations [5,6], and cell culture [7]. These and future approaches to high-level integration and automation with microfluidic devices have, and should continue, to reduce labor- and time-intensive steps in various analyses.

[*]Address Correspondence to: Dr. Michael G. Roper, Department of Chemistry and Biochemistry, Florida State University, 95 Chieftain Way, Dittmer Building, Tallahassee, FL 32306, USA, Ph 850-644-1846, Fx 850-644-8281, roper@chem.fsu.edu.

One important step to high-level integration and automation is fraction collection post-analysis; however, most of the work in sample preparation on microfluidic devices has focused on pre-analysis steps. These pre-analysis sample manipulations may be used to remove interfering components [8], enrich samples [9], or derivatize sample prior to separation [10]. Methods for automating post-analysis sample handling are far less common, with most reagents often sent to a "waste" reservoir merely to be disposed of after analysis. However, if a large number of steps were used to clean, enrich, or derivatize a sample, there may be a number of reasons one would wish to collect these samples after analysis. A simple method for isolating separated fractions on a microfluidic device would provide an attractive tool for continued development of increasingly complex integrated analysis systems.

Most fraction collection on microfluidic devices has been applied to gel-based electrophoretic separations [11–14]. These devices have demonstrated high efficiency size-based DNA separations, with one example demonstrating single base resolution [14]. However, as the majority of these devices used gel matrices, integration of these fraction collection schemes into other analysis systems requiring electroosmotic flow may not be possible

There have been fewer examples of fraction collection following free solution electrophoresis. In one example, the separation was collected comprehensively from a serpentine separation channel [15]. Although this device collected ten fractions, incorporation of this approach into amore complex integrated analysis system may be difficult as the device needed to be spun to induce a centrifugal force for fraction collection. In another example, a multilayer PDMS device was developed for isolating a single fraction during free solution electrophoresis [16]. Operation of this device required only manipulation of the applied electric potentials, which is ideal for automation. Although the method has the potential to collect more analytes, this multiplexing has not yet been demonstrated. In another example of a fraction collection device, a glass microfluidic chip was used to fractionate the effluent from an electrophoretic separation by switching the electric field from the separation channel to one of four outlet channels [17]. In this way, the analytes in the separation channel stopped while an eluted analyte was sent to one of these outlet channels where it was "parked" while separation recommenced. However, the contribution to band broadening which accompanied the removal of the electric field in the separation channel could be a significant disadvantage to this method of chip-based fraction collection. Although contamination between fractions was not observed, since there was no bulk flow in the outlet channels the opportunity existed for contamination between collected fractions by the diffusion of a collected band into the common intersection of the outlet channels.

To address the limitations of previous microfluidic fraction collection devices, we have developed a microfluidic chip that uses a continuous-flow fraction collection scheme. Electrokinetic focusing of the sample stream directed the separation effluent to one of seven collection channels. This type of focusing maintained a constant electric field in the separation channel while also maintaining a constant flow in the collection channels, thereby maintaining high separation efficiencies while minimizing the possibility of cross contamination. The geometry of the fluidic channels was optimized to minimize potential sources of fraction mixing, and to ensure that fractions were focused to a single collection channel without spillover into adjacent channels. Separation and isolation of fractions is demonstrated on a fluorescently-labeled amino acid mixture.

2. Materials and methods

2.1 Materials

Sodium tetraborate and hydrofluoric acid were purchased from Fisher Scientific (Pittsburgh, PA). Fluorescein isothiocyanate (FITC) was purchased from Sigma Aldrich (St. Louis, MO). Amino acids were purchased from MP Biomedicals (Solon, OH). HNO_3 was purchased from EMD Chemicals, Inc. (Gibbstown, NJ). All solutions were prepared in Mili-Q (Millipore, Bedford, MA) 18 MΩ·cm deionized water. Unless stated otherwise, all other chemicals were from Sigma Aldrich.

Electrophoretic separations were performed in a buffer consisting of 20 mM sodium tetraborate, pH 9.5. 100 µM FITC in separation buffer was used when imaging sample flow in the microfluidic device.

2.2 Simulations and Optimization

Electroosmotic flow and fluid transport were simulated using COMSOL Multiphysics (COMSOL Inc., Burlington, MA). The simulations were performed in two dimensions using geometric models representing the proportions of the microfluidic channels. The Conductive Media DC model was coupled with the Stokes Flow model to simulate electric field distribution and electroosmotic flow, respectively. The Stokes Flow model was then coupled to the Convection and Diffusion model to simulate mass transport. Each simulation was solved by finite element analysis over a simulation space of at least 40,000 elements using the direct UMFPACK solver. Design Expert 7 software (StatEase, Minneapolis, MN) was used in the optimization experiments to produce experimental designs and perform all statistical analyses.

2.3 Device Fabrication

The glass devices were fabricated by conventional photolithography and wet etching with hydrofluoric acid. A two-dimensional layout of the channel design was made using AutoCAD 2000 (Autodesk, Inc. San Rafeal, CA) and printed as a right-reading negative photomask on transparent film at a resolution of 16000 dpi (Fine Line Imaging, Colorado Springs, CO). Borofloat glass coated with chrome and positive phororesist (Telic Company, Valencia, CA), was covered by the photomask and exposed with a collimated UV source (OAI, San Jose, CA) for 5 seconds at an intensity of 20 mW cm^{-2} to sensitize the photoresist. After UV exposure, the sensitized photoresist was removed with AZ 400K Developer (AZ Electronic Materials Corp. Sommerville, NJ), and the underlying chrome was removed using a chrome etchant solution (CR-7S, Cyantek Corp. Fremont, CA) resulting in bare glass patterned in the two dimensional design of the fluidic channels. The exposed glass was then etched with a 66:14:20 (v:v:v) mixture of H_2O:HNO_3:HF under constant orbital shaking. Etched channel depths were verified to be 25 µm using a P-15 stylus profilometer (KLA-Tencor, Milpitas, CA) with a 2 µm diamond tipped stylus. Once etched, fluidic access holes were drilled and the remaining photoresist and chrome were removed. The etched substrates and borofloat cover slides were cleaned for 30 minutes in a 3:1 (v:v) solution of H_2SO_4:H_2O_2, followed by 30 minutes in a 5:1:1 (v:v:v) solution of H_2O:NH_4OH:H_2O_2. The cleaned substrates and cover slides were rinsed and placed between two 6 mm thick Macor slabs and pressed with a 2.5 kg steel weight while bonded at 640 °C for 8 hours.

Fluidic reservoirs were fabricated in a poly(methyl-methacrylate) manifold which sealed to the surface of the device using silicone o-rings and mechanical force provided by thumbscrews incorporated into the manifold design. 1 cm Pt electrodes were used to made electronic connections to the fluidic reservoirs.

2.4 Amino Acid Labeling

Amino acids were labeled with FITC using a reaction described elsewhere [18]. Arginine, glycine and glutamate were combined with FITC to a final concentration of 1 mM each amino acid and 100 µM FITC in a 20 mM sodium tetraborate buffer at pH 10.3. The reaction proceeded in darkness at room temperature for 12 h with constant agitation. The reaction mixture was then diluted 20-fold in separation buffer for use in electrophoretic separation experiments

2.5 Detection and Imaging

The microfluidic device was operated on the stage of a Nikon Eclipse Ti-S inverted fluorescence microscope (Nikon Instruments Inc., Mellville, NY). Epi-illumination was provided by a tungsten halogen lamp (model FOI 250, Techniquip, Pleasanton, CA). A filter cube (FITC-3540B, Semrock, Inc, Rochester, NY) contained an excitation band pass filter (488 ± 10 nm), emission bandpass filter (520 ± 10 nm) and a dichroic beam splitter to provide excitation light from the broadband light source and filter the fluorescence emission prior to detection. Images of fluid flow in the device were captured through a $10\times$ objective by a Cascade model EMCCD (Photometrics, Tucson, AZ). The CCD was coupled to the microscope using a coupler with a $0.38\times$ magnification lens (Optem SC38, Qioptiq LINOS, Inc. Fairport, NY). For separation experiments, fluorescence was excited by the 488 nm line of a 50 mW argon ion laser (Modulaser, Centerville, UT). Fluorescence intensity was measured through a 10X objective lens using a model D-104 photometer (Photon Technology International, Inc. Birmingham, NJ) which allowed for the adjustment of a spatial filter to define the region of interest prior to detection by a model R1527 photomultiplier tube (Hamamatsu Corp. Bridgewater, NJ).

2.6 Operation

Voltages for electrophoresis and electrokinetic focusing were generated using programmable high voltage power supplies, either model C50 (EMCO High Voltage Corporation, Sutter Creek, CA) or model 6AA12-P4 (Ultravolt, Ronkonkoma, NY). Switching of high voltages was performed using high voltage relays, models G81C245 and G81A245 (Gigavac, Santa Barbara, CA). Voltage programming was achieved using control software written in LabView 8.5 (National Instruments, Austin, TX).

During a separation, +2.75 kV was applied at both sample and buffer reservoirs while waste was grounded. As explained further in section 3.1, the sum of voltages at the sheath flow channels was +2.5 kV. To make an injection, the potential applied to the buffer reservoir was reduced to +1 kV while the voltage applied at the sheath flow channels was reduced to zero. Separation occurred when the applied potential at the buffer reservoir was returned to +2.75 kV and the total sheath flow voltage was returned to +2.5 kV. A similar modified gating procedure was reported previously [19].

3. Results and discussion

Previous examples [11–15,17] of microfluidic fraction collection devices required that the separation field be withheld while collecting fractions, a potential source of band broadening. Furthermore, in some of these devices, collected fractions were susceptible to cross-contamination by diffusion, since the collected bands were held stationary in close proximity to the common intersection of the collection channels. A recent report employed electrokinetic flow-switching in developing a chip-based serial-to-parallel fluidic interface [20]. We have employed a similar electrokinetic mechanism to develop a fraction collection device that operates in a continuous-flow format, without the need to withhold the separation field while collecting fractions.

3.1 Principle of operation

The microfluidic device, illustrated in Figure 1, introduced sample to the separation channel via a gated injection. Separation channel effluent was focused to one of seven fraction collection channels (C_1–C_7) by varying the ratio of potentials applied at the two sheath flow channels (Sf_1, Sf_2). To focus to the first and last fraction collection channel, two additional shaping channels (Sh) were necessary. Without these shaping channels, separation effluent being focused to C1 or C7 pooled in the adjacent sheath flow channel, since flow from this channel was greatly reduced.

There were two notable features of the microfluidic design that allowed its use as both an efficient separation device and a fraction collector. First, although the ratio of potentials at the sheath flow channels, $V_{sf1/sf2}$, changed depending on where the effluent was collected, the sum of the voltages applied to these reservoirs remained constant at +2.5 kV. This constant sheath flow voltage resulted in a constant electric field (275 V/cm) in the separation channel independent of which fraction collection channel was being used. Second, as the shaping and collection channels were always grounded, continuous flow from the sheath flow channels into the collection channels was maintained. As noted previously, these criteria of maintaining a constant flow in the separation and collection channels were features that were lacking in other reports but are beneficial to maintain peak efficiency and minimizing the potential for contamination between collection channels.

The separation effluent could be collected in all seven collection channels equally by sweeping the voltages at the sheath flow channels, or the effluent could be directed to any of the collection channels for a predetermined period of time by applying specific voltage ratios at the sheath flow channels.

3.2 Simulations and design optimization

Computer simulations of the flow profiles guided the device design. The parameters of the simulations are shown in Table 1 [19]. In the initial iterations of the device geometry, simulations demonstrated focusing of the separation channel effluent to a stream width occupying nearly 100% of a collection channel (Figure 2a). In Figure 2a, black indicates a simulated concentration of 100 µM fluorescein while white indicates a concentration of 0 µM. A more confined focus was desired to minimize the potential for spillover into adjacent fractions in the fabricated device. Also, when the sample stream was focused to C_1 or C_7, the separation effluent was pinched by the sheath flows resulting in the sample stream folding into the sheath flow channel closest to the collection channel where it was being focused and residing along the channel wall (Figure 2a). We deemed this folding to be undesirable as it could be a source of contamination between fractions.

To fully optimize the fraction collection device, a multivariate approach was used to: 1) minimize the length of separation effluent that resided along the wall of the sheath flow channel, L_{sf}, to minimize potential contamination with other fractions; 2) maximize the width of the flow profile at the separation channel exit, W_s, to maintain efficient separations and; 3) minimize the width of the flow profile at the entrance of the collection channel, W_c, again, to reduce the chance for contamination into adjacent collection channels. The microfluidic design factors that affected these three responses were found by intuition during various adjustments of the chip geometry in fluidic simulations. These factors are shown in Figure 2b, namely, the angle of intersection between sheath flow channels and the separation channel (θ) as well as the distance between the separation and collection channels (l). θ was varied over a range from 15° to 45°, and l varied from 0 to 800 µm.

Three different values of each of the two geometric factors were simulated (Table 2). ImageJ [21] was used to determine the three responses (L_{sf}, W_s, and W_c) from the 9 simulations. Each of these responses was then fit to a quadratic model that had the general equation:

$$Y=\beta_i+\theta+l+(\theta l)+\theta^2+l^2+E_i \qquad (1)$$

where Y was the response (L_{sf}, W_s, or W_c), β_i and E_i were the model coefficient and residual error, respectively, for each of the three responses. The term in parentheses was an interaction between factors, and squared terms were the quadratic effects of the factors. Analysis of variance (ANOVA) partitioned the total variation in the data into the variation due to the factors and to random error. Since the geometric parameters were changed in simulations, there was no random error, although this would not be the case in real experiments (see below). These components of variation were then used to calculate an F-value, a test statistic for the null hypothesis (no effect due to that factor). The calculated F-value was compared to a tabulated F-distribution to generate a result called "Prob>F" (p). If p was less than 0.05, then the effect of that factor was significant. Model reduction, which pooled non-significant terms (p > 0.10) with the residual error by backward elimination regression, was applied to find the best fit for each response. The final reduced model for each response was described by the following equations:

$$L_{sf}=\beta_1+\theta+l+\theta^2 \qquad (2)$$

$$W_s=\beta_2+\theta+l+\theta l \qquad (3)$$

$$W_c=\beta_3+\theta+l \qquad (4)$$

The ANOVA table for each response is shown in the Supplementary Information (Tables S1 – S3). As can be seen, each of these responses was dependent on θ and l with varying degrees of significance. Figures S1 – S3 in the Supplementary Information show the predicted results using these equations *vs.* the actual results obtained from simulations and as expected, results correlated well.

To combine these three responses into one overall score, each of these responses were weighted differently and combined into a final desirability score. The desirability score ranged from 0 (least desirable) to 1 (most desirable). A desirability of 1 would be achieved when L_{sf} was minimized, W_s was maximized, and W_c was ≤ 80% of the width of the collection channel to ensure flow would be isolated to a single collection channel. L_{sf} was weighted most heavily, since the potential it posed for contamination between bands was deemed most detrimental to the use of the device. Examination of multiple geometric configurations demonstrated focusing to individual fraction collection channels and therefore, W_c was of intermediate importance. W_s was given least weight, since the phenomenon this describes was least likely of the observed flow characteristics to adversely affect separation performance or the ability to isolate fractions. As seen in Figure 2c, a three-dimensional plot of desirability as a function of θ and l demonstrated the conditions that optimized L_{sf}, W_s and W_c. The optimal geometry was determined to be $\theta = 22.5°$ and $l = 350$ μm. A simulation of the most optimal device geometry is shown in Figure 2d.

A device of optimized geometry was fabricated and fluorescence images were taken to evaluate the agreement between simulations and the fabricated device. The trajectory of separation channel effluent as a function of $V_{sf1/sf2}$ (Figure 3 a–c) showed agreement with simulations, as did the width of the focused sample stream at the collection channel entrance (W_c) (for an example, compare Figures 2d and 3a). A sweep of $V_{sf1/sf2}$ values demonstrated that flow in the collection channels was continuous during device operation (Figure 3 d–f). The length of separation effluent residing on the sheath flow channel wall (L_{sf}) appeared greater in the fabricated device (~30 µm) as compared to simulations (10 µm). This deviation may have been due to differences between the two-dimensional simulation and electroosmotic flow in the three-dimensional channels of the device, to insignificant factors in the model being significant in real experiments, or to random experimental error. Ideally, the results from microfluidic experiments, not COMSOL simulations, would be used in the optimization of the geometric configurations. However, in our case, the ease of changing the geometry in simulations outweighed the advantages that the use of the microfluidic devices would have given. Regardless, the use of the optimized geometry provided complete isolation of the fractions while maintaining high separation efficiencies.

3.3 Device performance

To demonstrate the utility of the device in performing electrophoretic separations and fractionating separated bands, a mixture of FITC-conjugated amino acids was separated and the resulting components were isolated to one of four collection channels. An initial separation was performed and focused to C_4 (Figure 4a). From this separation, migration times of each peak were determined, which dictated the times when the sheath flow voltages were switched in subsequent separations. Repeated separations were performed with the sheath flow voltage ratios adjusted in time, as described in Table 3. In this way, each main peak would be fractioned to a different collection channel, C_1, C_3, C_5 and C_7, respectively. Fluorescence was monitored at the input of each of these collection channels for an entire separation to determine how well the peak of interest was isolated. As seen in Figure 4b, the data illustrated that the separated components were effectively isolated from one another to the limit of detection of the system. It can be seen from these individual traces that the background increased during the collection times and went back to a much lower value when the effluent was sent to a different collection channel. Furthermore, the agreement of migration times between the initial separation and the fractionated separations indicated that the magnitude of the electric field in the separation channel was unaffected by the value of the applied sheath flow voltage ratio, as expected from simulation results. This separation field cannot be increased by applying a higher separation voltage, since a higher separation voltage would require a higher sum of sheath flow voltages to achieve the same focus and the net effect on the separation field would be minimal.

4. Conclusion

This work has demonstrated an approach to chip-based fraction collection following free solution electrophoresis that incorporates several operational and design elements not addressed by previous devices. First, the device collects fractions without stopping the electrophoretic separation, which is advantageous in that it minimizes diffusional band broadening during the separation. Second, fractions are collected in a continuous-flow format that eliminates the possibility of cross contamination of collected bands by diffusion. Third, this device has the capacity to collect numerous fractions using a relatively simple electronic configuration, as all collection channels are grounded. Further development on this system will be aimed at redesigning the fluidic architecture to allow for greater separation fields.

Supplementary Material

Refer to Web version on PubMed Central for supplementary material.

Acknowledgments

References

1. Duraiswamy S, Khan SA. Small. 2009; 5:2828–2834. [PubMed: 19787681]

2. Mellors JS, Jorabchi K, Smith LM, Ramsey JM. Anal. Chem. 2010; 82:967–973. [PubMed: 20058879]

3. Easley CJ, Karlinsey JM, Bienvenue JM, Legendre LA, Roper MG, Feldman SH, Hughes MA, Hewlett EL, Merkel TJ, Ferrance JP, Landers JP. Proc. Natl. Acad. Sci. U. S. A. 2006; 103:19272–19277. [PubMed: 17159153]

4. Reid KR, Kennedy RT. Anal. Chem. 2009; 81:6837–6842. [PubMed: 19621896]

5. Wen J, Wilker EW, Yaffe MB, Jensen KF. Anal. Chem. 2010; 82:1253–1260. [PubMed: 20092256]

6. Turgeon RT, Bowser MT. Anal. Bioanal. Chem. 2009; 394:187–198. [PubMed: 19290514]

7. Gomez-Sjoberg R, Leyrat AA, Pirone DM, Chen CS, Quake SR. Anal. Chem. 2007; 79:8557–8563. [PubMed: 17953452]

8. Roper MG, Frisk ML, Oberlander JP, Ferrance JP, McGrory BJ, Landers JP. Anal. Chim. Acta. 2006; 569:195–202.

9. Ramsey RS, Ramsey JM. Anal. Chem. 1997; 69:1174–1178.

10. Jacobson SC, Hergenroder R, Moore A, Ramsey JM. Anal. Chem. 1994; 66:4127–4132.

11. Khandurina J, Chovan T, Guttman A. Anal. Chem. 2002; 74:1737–1740. [PubMed: 12033268]

12. Lin R, Burke DT, Burns MA. J. Chromatogr., A. 2003; 1010:255–268. [PubMed: 12974295]

13. Li G, Ran R, Zhao J, Xu Y. Electrophoresis. 2007; 28:4661–4667. [PubMed: 18004713]

14. Sun K, Suzuki N, Li Z, Araki R, Ueno K, Juodkazis S, Abe M, Noji S, Misawa H. Electrophoresis. 2009; 30:4277–4284. [PubMed: 20013913]

15. Spesny M, Foret F. Electrophoresis. 2003; 24:3745–3747. [PubMed: 14613200]

16. Tulock JJ, Shannon MA, Bohn PW, Sweedler JV. Anal. Chem. 2004; 76:6419–6425. [PubMed: 15516136]

17. Zalewski D, Schlautmann S, Schasfoort R, Gardeniers H. Lab Chip. 2008; 8:801–809. [PubMed: 18432352]

18. Cheng Y, Dovichi N. Science. 1988; 242:562–564. [PubMed: 3140381]

19. Lerch MA, Jacobson SC. Anal. Chem. 2007; 79:7485–7491. [PubMed: 17718538]

20. Zhuang Z, Jacobson SC. Anal. Chem. 2009; 81:1477–1481. [PubMed: 19152307]

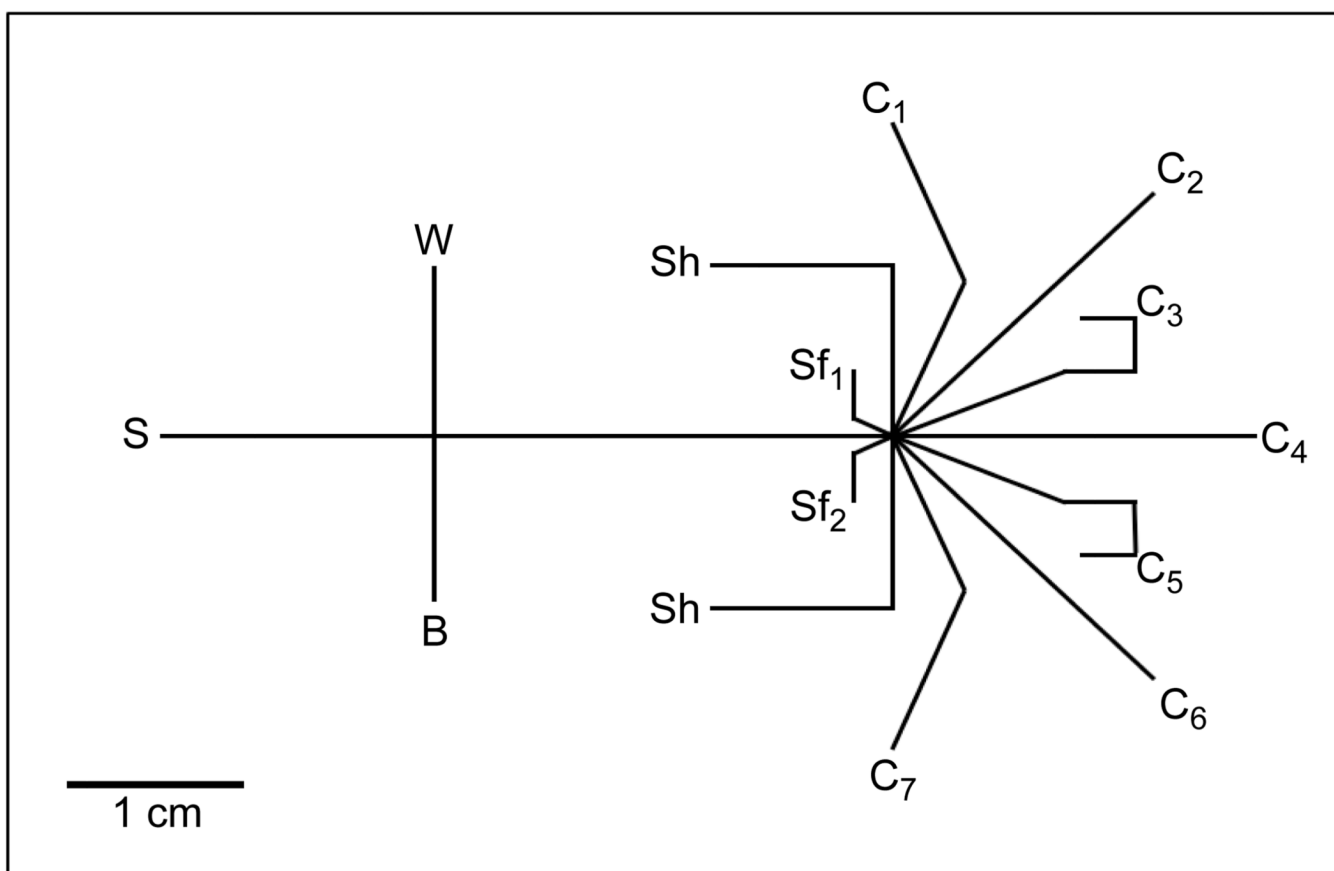21. Abramoff MD, Magelhaes PJ, Ram SJ. Biophotonics International. 2004; 11:36–42.

Figure 1. Schematic of the microfluidic device
Sample (S) was introduced to the separation channel by a gated injection at the intersection of S, buffer (B) and waste (W) channels. Sheath flow channels (Sf_1, Sf_2) focused separation channel effluent to one of seven fraction collection channels (C_1–C_7). Flow shaping channels (Sh) were employed to maintain focusing when sample was directed to C_1 or C_7.
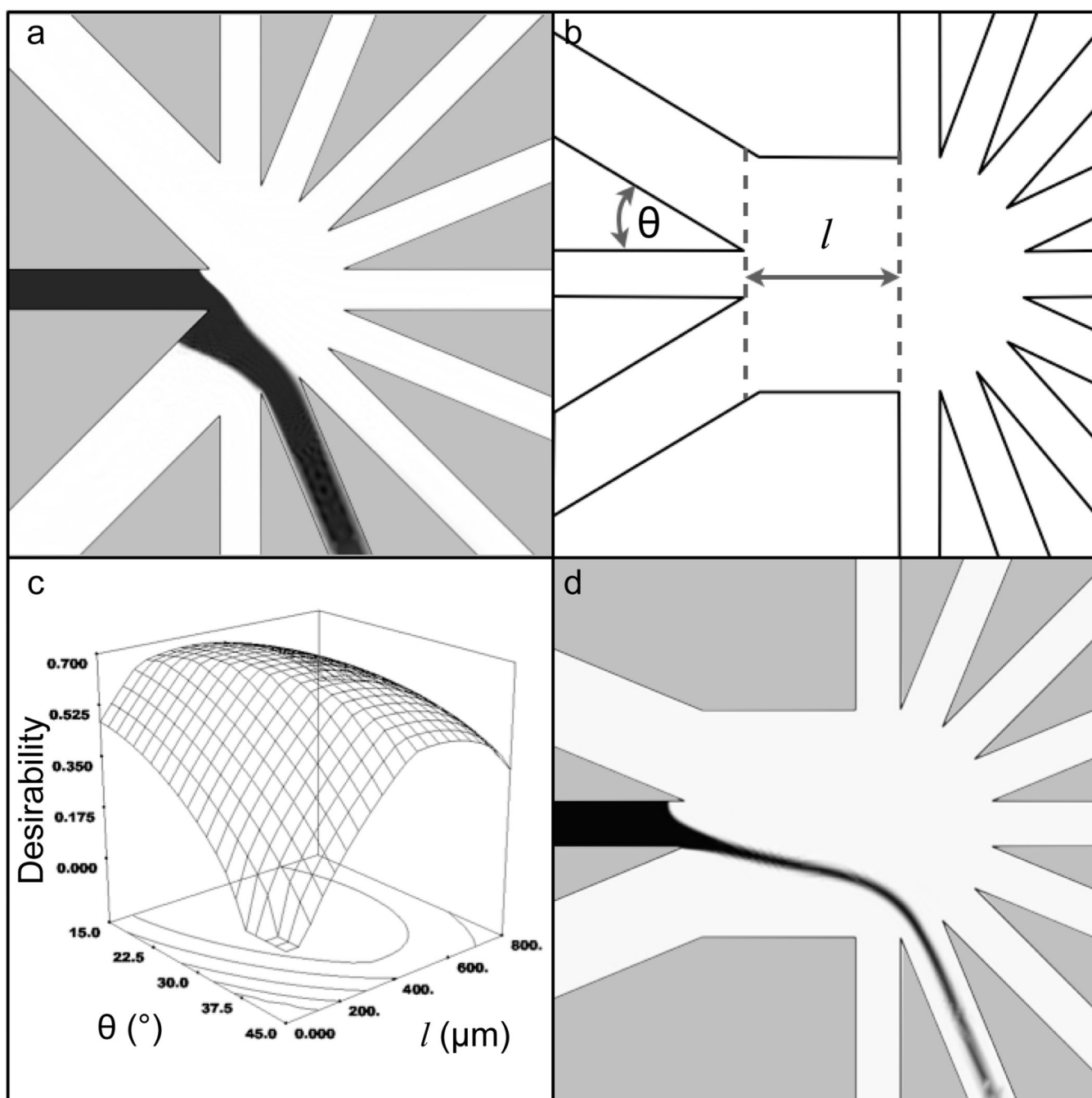
Figure 2. Optimization of device geometry
a. Early simulations demonstrated poorly confined sample focusing and flow residing on the sheath flow channel wall. Black to white gradient represents a simulated concentration gradient from 100 µM to 0 µM fluorescein respectively. **b**. In simulations, sheath flow angle (θ) and focus channel length (*l*) were shown to affect the flow profile of the focused sample stream. **c**. A surface plot showing the desirability of the flow characteristics as a function of θ and *l* indicated an optimal geometry of θ = 22.5° and *l* = 350 µm **d**. A simulation of the optimal device geometry.
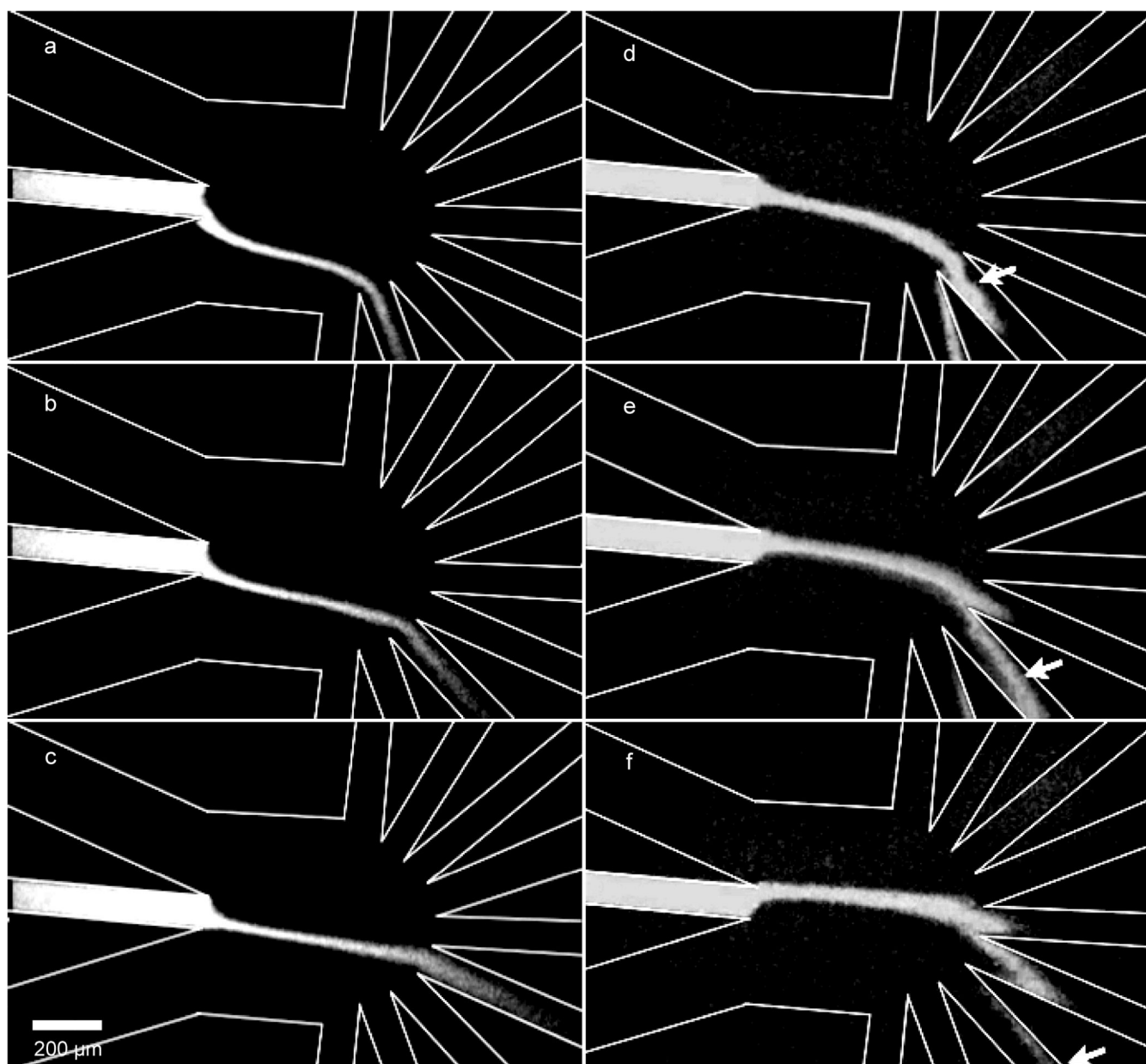
Figure 3. Fluorescence micrographs of fluid flow in the device
a. $V_{sf1/sf2} = 1.27$ **b**. $V_{sf1/sf2} = 1.17$ **c**. $V_{sf1/sf2} = 1.08$ **d–f**. As indicated by the arrows, a plug can be seen migrating into the collection channels demonstrating that the device operated with continuous flow in the these channels.
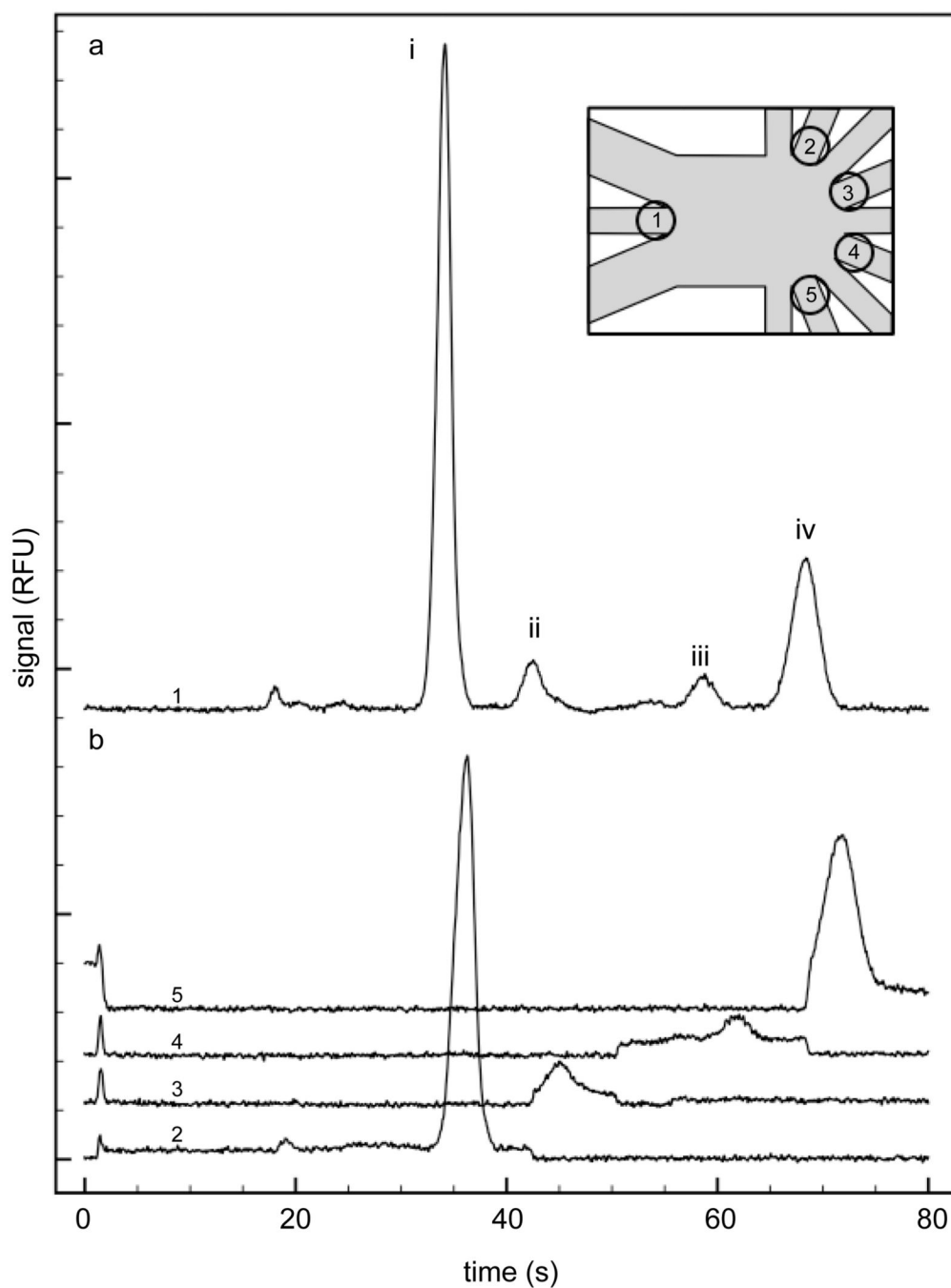
Figure 4. FITC-conjugated amino acid separation and isolation
a. During the initial separation, the entire separation was sent to C$_4$. Peak identities are (i) FITC-arginine, (ii) FITC, (iii) FITC-glycine, (iv) FITC-glutamate. **b**. The fluorescence was monitored at the opening of each collection channel during subsequent separations using the timing protocol shown in Table 3. The inset indicates the detection spots for the corresponding traces in **a** and **b**.

Table 1

Parameters used in COMSOL simulations

Viscosity (η)	1×10^{-3} Pa s
Density (ρ)	1×10^{3} kg m^{-1}
Electrical Conductivity (σ)	1.5×10^{-2} S m^{-1}
Zeta Potential (ζ)	-5×10^{-2} V
Diffusion Coefficient (D)	6.7×10^{-10} m^2 s^{-1}
Concentration (c)	1 mol m^{-3}

Table 2

Experimental factors and levels used in the three level factorial design

Factors	Level (−)	Level (0)	Level (+)
Focus Channel length (l, µm)	0	400	800
Sheath Flow intersection angle (θ, °)	15	30	45

Table 3

Timed voltage parameters for amino acid fraction collection

Collection window	$V_{sf1/sf2}$	Collection channel
0 – 42 s	0.78	C_1
42 – 50 s	0.92	C_3
50 – 68 s	1.08	C_5
68 – 80 s	1.27	C_7